The Astrophysical Journal Letters, 803:L19 (7pp), 2015 April 20 doi:10.1088/2041-8205/803/2/L19

VERTICAL DISTRIBUTION OF C_3-HYDROCARBONS IN THE STRATOSPHERE OF TITAN

Cheng Li[1], Xi Zhang[2], Peter Gao[1], and Yuk Yung[1]
[1] Division of Geological and Planetary Science, California Institute of Technology, Pasadena, CA 91125, USA
[2] Lunar and Planetary Laboratory, University of Arizona, Tucson, AZ 85721, USA
Received 2015 January 9; accepted 2015 March 23; published 2015 April 15

ABSTRACT

Motivated by the recent detection of propene (C_3H_6) in the atmosphere of Titan, we use a one-dimensional Titan photochemical model with an updated eddy diffusion profile to systematically study the vertical profiles of the stable species in the C_3-hydrocarbon family. We find that the stratospheric volume mixing ratio of propene (C_3H_6) peaks at 150 km with a value of 5×10^{-9}, which is in good agreement with recent observations by the Composite Infrared Spectrometer on the *Cassini* spacecraft. Another important species that is currently missing from the hydrocarbon family in Titan's stratosphere is allene (CH_2CCH_2), an isomer of methylacetylene (CH_3C_2H). We predict that its mixing ratio in the stratosphere is about 10^{-9}, which is on the margin of the detection limit. CH_2CCH_2 and CH_3C_2H equilibrate at a constant ratio in the stratosphere by hydrogen-exchanging reactions. Thus, by precisely measuring the ratio of CH_2CCH_2 to CH_3C_2H, the abundance of atomic hydrogen in the atmosphere can be inferred. No direct yield for the production of cyclopropane (c-C_3H_6) is available. From the discharge experiments of Navarro-González & Ramírez, the abundance of cyclopropane is estimated to be 100 times less than that of C_3H_6.

Key words: astrochemistry – planets and satellites: atmospheres – planets and satellites: composition – planets and satellites: individual (Titan)

1. INTRODUCTION

Titan's atmosphere is laden with hundreds of interacting hydrocarbon species, which group in families according to the number of carbon atoms in their hydrocarbon chains (i.e., C_1-, C_2-, C_3-hydrocarbon, etc.). Many simple hydrocarbon molecules (C_1- and C_2-hydrocarbons) have been found by spectroscopic and mass spectrometric measurements of Titan's atmosphere (Coustenis et al. 2003, 2007; Vuitton et al. 2007; Magee et al. 2009). They have also been the subject of extensive investigations in previous photochemical models (Yung et al. 1984; Wilson & Atreya 2004, 2009; Lavvas et al. 2008a; Krasnopolsky 2009; Vuitton et al. 2012; Hebrard et al. 2013). Recently, analysis of *Cassini*/Composite Infrared Spectrometer (CIRS) limb-viewing observations (Nixon et al. 2013) identified a peak in the infrared spectrum of Titan's stratosphere at 912.5 cm^{-1}, which is attributed to the ν_{19} band of propene (C_3H_6). By comparing the relative emission strengths of propene and propane (C_3H_8), the stratospheric vertical profile of C_3H_6 is retrieved. This observation provides a new constraint for the photochemical modeling of Titan's atmosphere and fills a gap in the C_3-hydrocarbon family. As Nixon et al. (2013) pointed out, even though the five C_3 molecules (the two isomers of C_3H_4, allene and methylacetylene; the two isomers of C_3H_6, propene and cyclopropane; and propane) are part of the interwoven net of hydrocarbon species in the atmosphere of Titan, allene (CH_2CCH_2) and cyclopropane (c-C_3H_6) are yet to be detected. Roe et al. (2011) tentatively identified several of the ν_{10} sub-bands of allene among the strong emission lines of ethane's ν_{12} band using TEXES (Texas Echelon Cross Echelle Spectrograph) at NASA/IRTF. However, due to the large uncertainties in the laboratory spectra of allene, measuring its abundance in Titan's atmosphere by comparing laboratory and observed spectra is difficult.

In this Letter, we use the Caltech/JPL photochemical model with a recently updated eddy diffusion profile (Li et al. 2014) to explain the observed vertical distribution of propene. We also perform a systematic study of C_3-hydrocarbon chemistry focusing on CH_3C_2H (methylacetylene), CH_2CCH_2 (allene), C_3H_6 (propene), and c-C_3H_6 (cyclopropane). Our photochemical model gives improved results that, for the first time, fit the abundances of all observable hydrocarbons, which is a significant advance over previous works (Yung et al. 1984; Wilson & Atreya 2004; Lavvas et al. 2008b; Vuitton et al. 2012; Hebrard et al. 2013; Krasnopolsky 2014).

In Section 2, we describe the photochemical model and compare the modeling results for C_1- and C_2-hydrocarbons to the observations. In Section 3, we examine the vertical profile of C_3H_6 and its production/loss pathways. In Section 4, we discuss how the relative abundance of two isomers, CH_2CCH_2 and CH_3C_2H, is a strong tracer of atomic H in the atmosphere. In Section 5, we estimate the abundance of c-C_3H_6, another missing C_3-hydrocarbon. In Section 6, we state our conclusions.

2. PHOTOCHEMICAL MODEL AND C_2-HYDROCARBONS

The Caltech/JPL one-dimensional photochemical model for Titan solves the mass continuity equation from 50 to 1500 km in altitude:

$$\frac{\partial n_i}{\partial t} + \frac{\partial \psi_i}{\partial z} = P_i - L_i, \quad (1)$$

where n_i, P_i, and L_i are the number density and chemical production and loss rates of species i, respectively. ψ_i is the

vertical flux of species i calculated from the equation:

$$\psi_i = -\frac{\partial n_i}{\partial z}\left(D_i + K_{zz}\right) - n_i\left(\frac{D_i}{H_i} + \frac{K_{zz}}{H_a}\right) - n_i\frac{\partial T}{\partial z}\frac{\left(1+\alpha_i\right)D_i + K_{zz}}{T}, \quad (2)$$

where D_i and H_i are the molecular diffusion coefficient and scale height of species i, respectively; H_a is the atmospheric scale height; α_i is the thermal diffusion coefficient of species i, T is the temperature, and K_{zz} is the eddy diffusion coefficient. The K_{zz} vertical profile is similar to that of (Li et al. 2014) but simplified using a log-linear interpolation of four nodal levels at $z_1 = 120$ km, $z_2 = 300$ km, $z_3 = 500$ km and $z_4 = 1000$ km:

$$\log K_{zz}(z) = \begin{cases} \log\left(3\times10^3\right), & z < z_1 \\ \log\left(3\times10^3\right)\dfrac{z_2 - z}{z_2 - z_1} + \log\left(2\times10^7\right)\dfrac{z - z_1}{z_2 - z_1}, & z_1 \leqslant z \leqslant z_2 \\ \log\left(2\times10^7\right)\dfrac{z_3 - z}{z_3 - z_2} + \log\left(2\times10^6\right)\dfrac{z - z_2}{z_3 - z_2}, & z_2 \leqslant z \leqslant z_3 \\ \log\left(2\times10^6\right)\dfrac{z_4 - z}{z_4 - z_3} + \log\left(4\times10^8\right)\dfrac{z - z_3}{z_4 - z_3}, & z_3 \leqslant z \leqslant z_4 \\ \log\left(4\times10^8\right), & z \geqslant z_4 \end{cases} \quad (3)$$

We use pure absorbing aerosols with extinction cross sections independent of wavelength to account for absorption of UV radiation (Li et al. 2014). The particle size and density as a function of altitude are taken from (Lavvas et al. 2011). Their cross sections are scaled so that the line-of-sight aerosol optical depth matches the *Cassini*/UVIS measurements (Koskinen et al. 2011) at 400–600 km ($\sim 10^{-2}$). The thermosphere density profile uses the measurements from *Cassini*/INMS during the T40 flyby (Westlake et al. 2011). The stratospheric density profile is interpolated from *Cassini*/HASI (Fulchignoni et al. 2005). The mesospheric density profile is extrapolated from the thermospheric density profile assuming constant temperature until it connects to the stratospheric profile. The chemical reactions are taken from (Moses et al. 2005) with adjusted reaction rates for $H + C_2H_4 \xrightarrow{M} C_2H_5$ as recommended by (Li et al. 2014). CH_4 does not escape from the top of the atmosphere because applying an escaping flux to CH_4 has the same effect as applying a larger eddy diffusivity (Yelle et al. 2008). We prefer the second approach because it improves to fits to the ^{40}Ar profile, as seen in Figure 11 of Li et al. (2014). We refer the reader to Li et al. (2014) for more details regarding the model.

Figure 1 compares the vertical distributions of CH_4, C_2H_2, C_2H_4, and C_2H_6 with the recent observations from *Cassini*/CIRS (Vinatier et al. 2010), *Cassini*/UVIS (Koskinen et al. 2011; Kammer et al. 2013), and *Cassini*/INMS (Magee et al. 2009). The observations show a near-constant mixing ratio for C_2H_2 and C_2H_6 in the stratosphere, above which the mixing ratios increase gradually until reaching their peak values near 1000 km. C_2H_4 is an exception to this rule. In some flybys, its mixing ratio significantly decreases with altitude. Our model does not reproduce this feature. This is probably due to two-dimensional effects, such as horizontal advection and mean upwelling/subsidence, which are not included in the one-dimensional model. However, on average our model profiles of CH_4 and C_2-hydrocarbons are able to match the mean measurements between flybys satisfactorily, and can thus serve as the basis for our study of C_3-hydrocarbons.

3. PROPENE (C_3H_6) VERTICAL DISTRIBUTION

The mixing ratios of the C_3-hydrocarbons C_3H_6, CH_2CCH_2, CH_3C_2H, and C_3H_8 are shown in Figure 2. The observed stratospheric mixing ratio of C_3H_6 peaks at 200 km with a value of 5×10^{-9}. Our model reproduces a similar peak value and the peaked structure at 150 km. The modeled mixing ratio of C_3H_6 at 1000 km is two times less than the observed value from *Cassini*/INMS. There are two possible reasons that might explain this discrepancy. First, the thermosphere of Titan exhibits large natural variability as observed by multiple *Cassini* flybys, e.g., Figure 2 of Westlake et al. (2011), while our photochemical model represents the mean atmospheric condition, which might deviate from individual measurements by *Cassini*/INMS. In fact, the abundances of the C_3-hydrocarbons in our model all tend to deviate from the *Cassini*/INMS measurements by within a factor of two. The magnitude of the deviation agrees with the spread in thermospheric density profiles retrieved from different flybys. Second, our current photochemical model does not include the radiative association reaction: $H + C_3H_5 \rightarrow C_3H_6$, which may double the current production rate of C_3H_6 at 1000 km (Hebrard et al. 2013). We estimate this effect by doubling the reaction rate of the key reaction identified in the next paragraph and the results show an improved fit to *Cassini*/INMS.

The reaction rates of the C_3-hydrocarbons and their errors have been studied extensively (Hebrard et al. 2013; Loison et al. 2015). However, systematic analyzes of their formation/loss pathways are limited because of the formidable quantity of reactions involved. In this work, we use a greedy algorithm that traverses the complete reaction list to find the subset of reactions that contribute to over 90% of the total formation and loss of a certain species over all altitudes. Reactions with larger rates are preferred to be added in the subset than ones with smaller rates. Figure 3 shows the production and loss pathways of C_3H_6 produced by this algorithm. In the upper atmosphere (>600 km), the production of C_3H_6 is dominated by the insertion of CH radicals into C_2H_6:

$$CH + C_2H_6 \rightarrow C_3H_6 + H, \quad (4)$$

where the CH radicals are produced by the photodissociation of CH_4. By contrast, Hebrard et al. (2013) includes the radiative association reaction:

$$H + C_3H_5 \rightarrow C_3H_6, \quad (5)$$

which makes up 61.8% of the production of C_3H_6 at 1000 km while Reaction (4) contributes 36.7%. Currently we do not have this reaction in our photochemical model. However we estimate its effect by doubling the reaction rate of (4). As a result, the abundance of C_3H_6 increases by a factor of two and matches the *Cassini*/INMS observations. In the intermediate altitudes ($300\sim600$ km), where the CH radicals are rare and

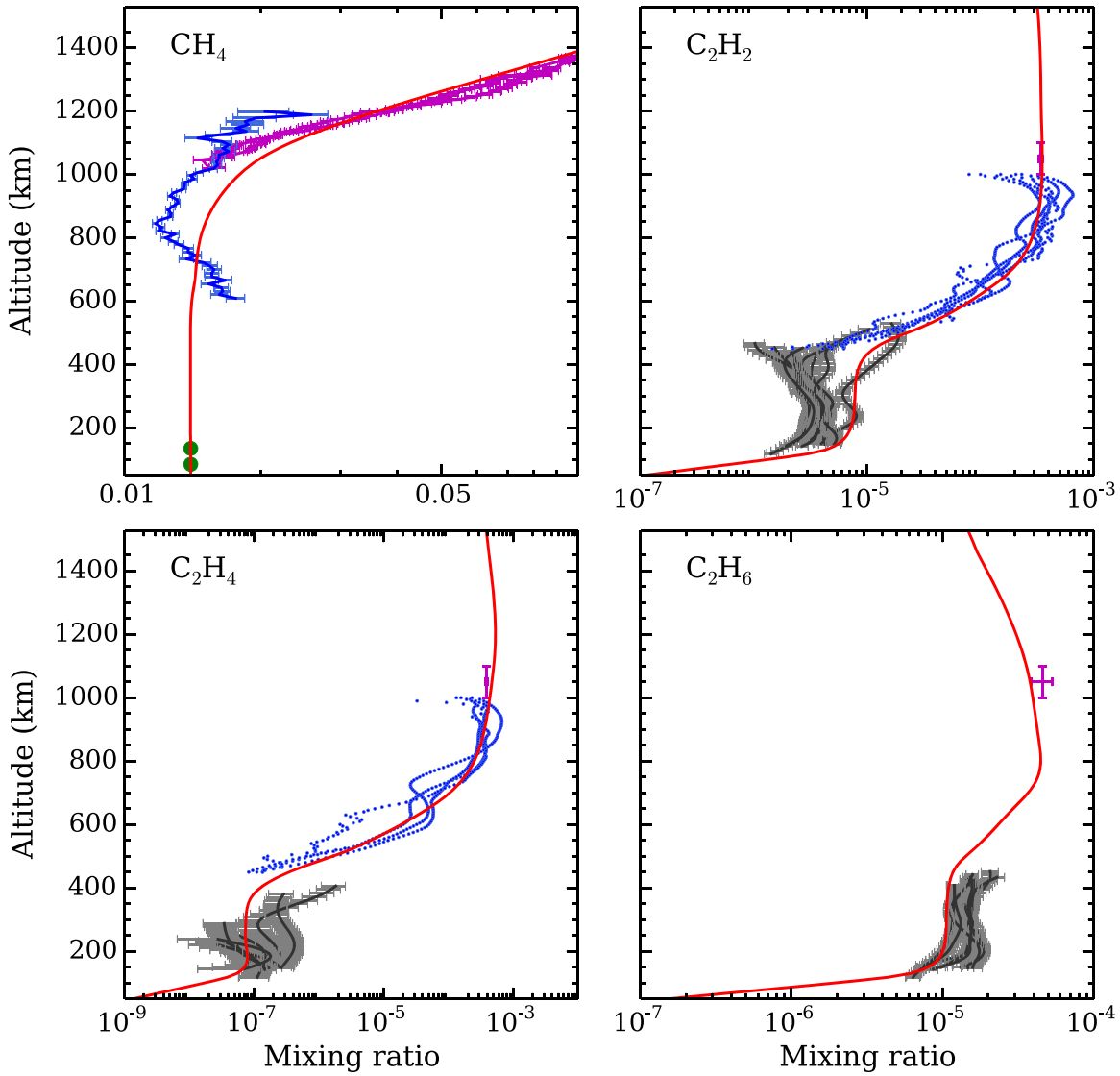

Figure 1. The mixing ratios of CH_4 and three C_2-hydrocarbons C_2H_2, C_2H_4, and C_2H_6. Our model results are shown in red. The *Cassini*/INMS measurements are displayed as magenta dots: CH_4 is from the T40 *Cassini* flyby (Westlake et al. 2011); the others are from Magee et al. (2009). The *Cassini*/UVIS stellar occultation measurements (Koskinen et al. 2011; Kammer et al. 2013) are displayed as blue dots. The *Cassini*/CIRS limb view observations (Vinatier et al. 2010) are displayed as black dots. The Huygens/GCMS in situ measurements (Niemann et al. 2005) for CH_4 are shown as green dots.

where the pressure is too low to drive termolecular combination, photodissociation of C_3H_8 is the dominant process in the production of C_3H_6:

$$C_3H_8 + h\nu \rightarrow C_3H_6 + H_2. \quad (6)$$

In the stratosphere (<300 km) where the pressure is high, the three-body reaction

$$CH_3 + C_2H_3 + M \rightarrow C_3H_6 + M, \quad (7)$$

becomes the dominant production pathway of C_3H_6 and creates the local peak in the mixing ratio, as shown in Figure 2. Though the production of C_3H_6 peaks at 200 km, our model produces the abundance peak 50 km lower. This is probably due to eddy mixing effects, as the value of the eddy diffusivity at 200 km is 2×10^6 cm^2 s^{-1}, the chemical loss time scale for C_3H_6 at 200 km is 2×10^7 s, and so the expected dynamic mixing length is $\delta = \sqrt{2 \times 10^6 \times 2 \times 10^7}$ cm ≈ 60 km. CH_3 in Reaction (7) comes from the photosensitized dissociation of CH_4 in the stratosphere (Yung et al. 1984) by

$$C_2H_2 + h\nu \rightarrow C_2H + H \quad (8)$$

$$C_2H + CH_4 \rightarrow CH_3 + C_2H_2. \quad (9)$$

C_2H_3 in Reaction (7) comes from the three-body reaction:

$$H + C_2H_2 + M \rightarrow C_2H_3 + M. \quad (10)$$

Therefore, the abundance of C_3H_6 in the stratosphere is directly related to the abundance of C_2H_2. Other models fail to produce the abundance of C_3H_6 because they underestimate the stratospheric abundance of C_2H_2 (Wilson & Atreya 2004, 2009; Krasnopolsky 2010; Vuitton et al. 2012; Hebrard et al. 2013). C_3H_6 is destroyed mainly through photolysis:

$$C_3H_6 + h\nu \rightarrow \alpha(C_3H_5 + H) + \beta(C_2H_3 + CH_3), \quad (11)$$

where $\alpha \approx 0.6$, $\beta \approx 0.4$ are the branching ratios of the photolysis reaction. C_3H_6 can also be destroyed by reacting

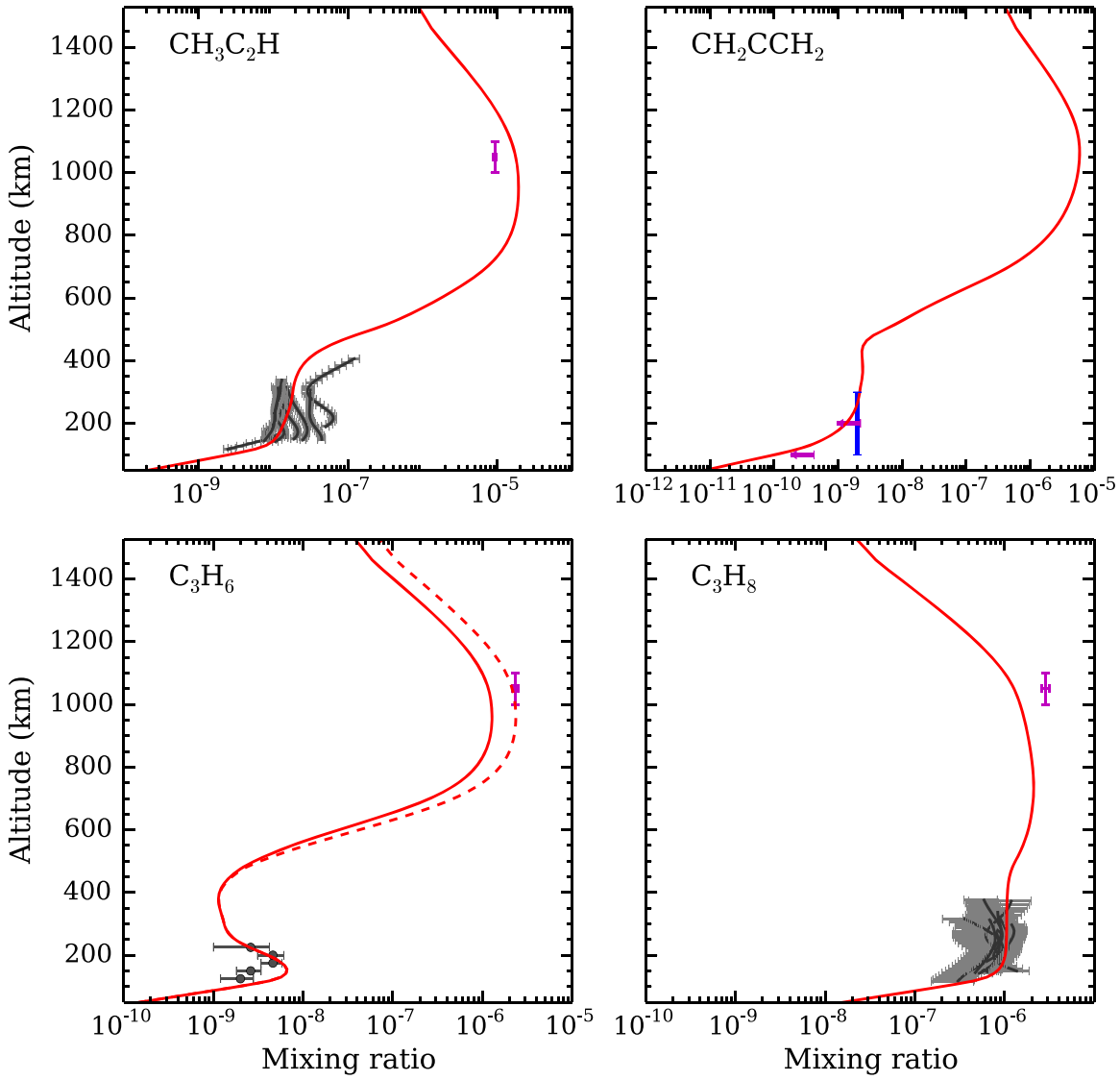

Figure 2. Same as Figure 1, but for C_3-hydrocarbons. Blue bar in CH_2CCH_2 panel indicates the upper limit by Coustenis et al. (2003); magenta points with arrows in CH_2CCH_2 panel indicate the upper limit by Nixon et al. (2010). Dashed red line in C_3H_6 panel shows the profile when the reaction rate of $CH + C_2H_6 \rightarrow C_3H_6 + H$ is doubled.

with an H atom:

$$H + C_3H_6 + M \rightarrow C_3H_7 + M. \quad (12)$$

The rate of this three-body reaction increases with atmospheric density and becomes greater than the photo-dissociation reaction rate below 300 km (as shown in Figure 3).

4. ALLENE (CH_2CCH_2) TO METHYLACETYLENE (CH_3C_2H) RATIO AS A PROBE OF H ATOM ABUNDANCE

Allene (CH_2CCH_2, or propadiene) and methylacetylene (CH_3C_2H, or propyne) are isomers. Goulay et al. (2009) reported the following branching ratios:

$$CH + C_2H_4 \rightarrow CH_2CCH_2 + H \quad (70\%) \quad (13)$$

$$\rightarrow CH_3C_2H + H \quad (30\%). \quad (14)$$

The enthalpy difference between CH_3C_2H and CH_2CCH_2 is $\sim$1 kcal mol^{-1} (Rogers & Mclafferty 1995). Because it takes very little energy to convert between CH_3CH_2 and CH_2CCH_2, their production and loss rates are expected to be comparable. Using the same algorithm in Section 3, their major production and loss pathways are calculated and presented in Figure 4. In the upper atmosphere, CH_3C_2H and CH_2CCH_2 originate from C_2H_4 and C_3H_5 through

$$CH + C_2H_4 \rightarrow CH_3C_2H/CH_2CCH_2 \quad (15)$$

$$H + C_3H_5 \rightarrow CH_3C_2H/CH_2CCH_2 + H_2 \quad (16)$$

$$CH_3 + C_3H_5 \rightarrow CH_3C_2H/CH_2CCH_2 + CH_4. \quad (17)$$

Reaction (15) terminates near 600 km due to CH_4 self-shielding reducing the production rate of CH radicals. Reactions (16) and (17) persist throughout the entire atmosphere because H atoms and CH_3 are replenished in the lower atmosphere by photosensitized dissociation of CH_4. Reactions (16) and (17) both lead to the same production rate for CH_3C_2H and CH_2CCH_2, so to explain the non-detection of

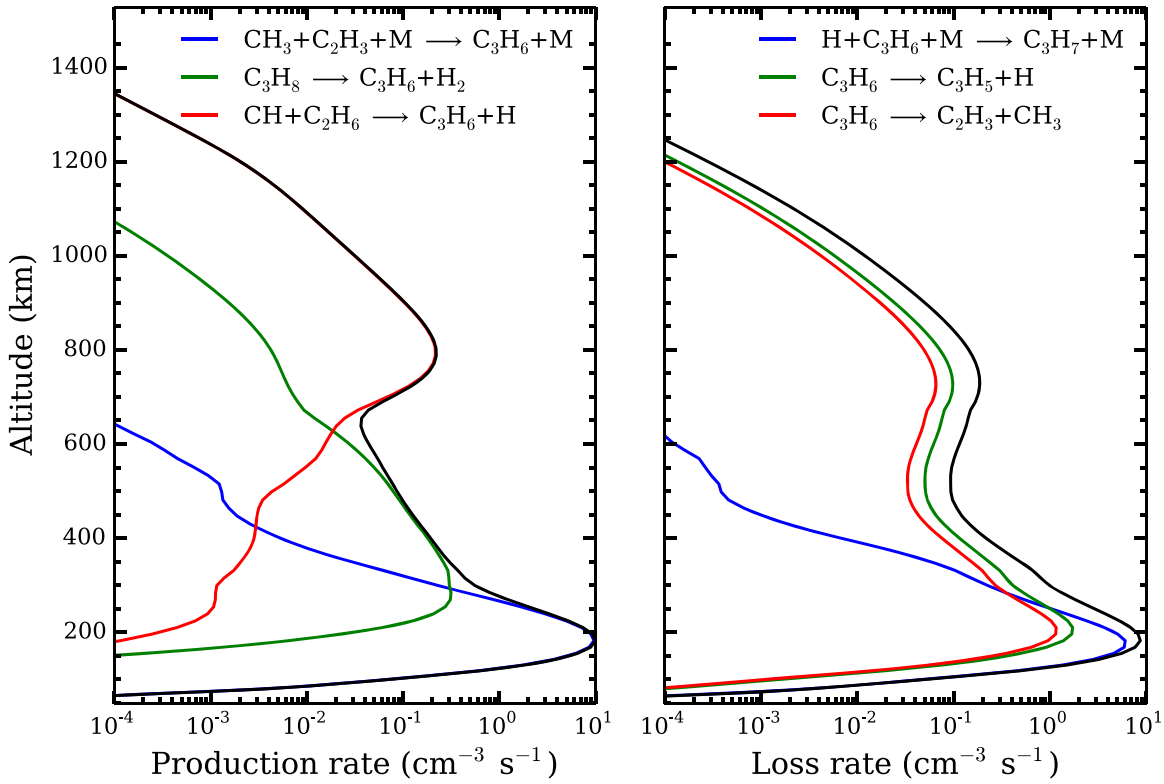

Figure 3. Production (left) and loss rates (right) of C_3H_6 due to reactions listed in the figure. The sum of the reactions accounts for more than 90% of the total production and loss rates at each altitude. The total production and loss rates are given by the black lines.

CH_2CCH_2 Yung et al. (1984) proposed an exchange reaction:

$$H + CH_2CCH_2 \rightarrow CH_3C_2H + H, \quad (18)$$

which is exothermic by ~1.6 kcal mol^{-1}. As a result of this exchange reaction, the abundance of CH_2CCH_2 is significantly less than that of CH_3C_2H and their relative abundance equilibrates at a constant ratio as a function of the abundance of H atom. Figure 5 shows the correlation between the mixing ratios of CH_2CCH_2 and CH_3C_2H at several altitudes, as labeled on the correlation curve. From 50 to 800 km, the mixing ratio of CH_2CCH_2 is equal to 0.2 times that of CH_3C_2H, aside from 150 to 350 km where the abundance of CH_2CCH_2 increases. The equilibration is a highly sensitive function of the H concentration in the atmosphere, as demonstrated by cracking reactions that can reverse the process of organic synthesis, e.g., Yung et al. (1984). We performed four experiments to investigate the hydrogenation process (Sekine et al. 2008a, 2008b), each with a different accommodation coefficient (0, 0.001, 0.01, and 0.1) of H atoms on aerosol particles. As shown in Figure 5, the concentration of H atoms in the atmosphere can be inferred from the CH_2CCH_2 to CH_3C_2H ratio, as larger concentrations of H result in lower concentrations of CH_2CCH_2.

Roe et al. (2011) discussed the challenges of measuring allene in the atmosphere of Titan using extremely high resolution ground-based spectra near 845 cm^{-1} to separate allene lines from ethane lines (this possibility was demonstrated in the upper panel of Figure 12 of Coustenis et al. 2003). An upper limit of ~10^{-9} was found, which is an order of magnitude less than that of CH_3C_2H. Nixon et al. (2010) obtained 3σ upper limits for allene of 0.3×10^{-9} at 100 km and 1.6×10^{-9} at 200 km using *Cassini*/CIRS. Our model predicts an allene mixing ratio of ~10^{-9} at 200 km, which increases to ~2×10^{-9} at 400 km. These values are consistent with the previous studies and could be confirmed by further measurements given better laboratory spectra. Precise measurements of allene will offer a unique opportunity to probe a very sensitive but hitherto unobserved part of the atmospheric chemistry of Titan.

5. ESTIMATED ABUNDANCE OF CYCLOPROPANE (c-C_3H_6)

Figure 1 of Nixon et al. (2013) raises the possibility of c-C_3H_6, which is an isomer of propene. This molecule has not been detected in the atmosphere of Titan. Reaction (4) primarily produces C_3H_6, while the branch producing the isomer c-C_3H_6 is considered exceedingly slow (Galland et al. 2003). No published yield for c-C_3H_6 is available, though we can estimate a yield ~1% relative to C_3H_6 or C_3H_8 from the discharge experiments of Navarro-González & Ramírez (1997). Thus, we would estimate c-C_3H_6 concentrations in the atmosphere of Titan to be a hundred times less than that of C_3H_6.

6. CONCLUSIONS

Our model reproduced the abundances of C_2-hydrocarbons and the newly observed C_3H_6 in the atmosphere of Titan. The model also shows that CH_2CCH_2 is in equilibrium with its isomer CH_3C_2H by a constant ratio, which is a strong function of the abundance of H atoms in the atmosphere. The abundance of CH_2CCH_2 is close to the detection limit, and so it is possible

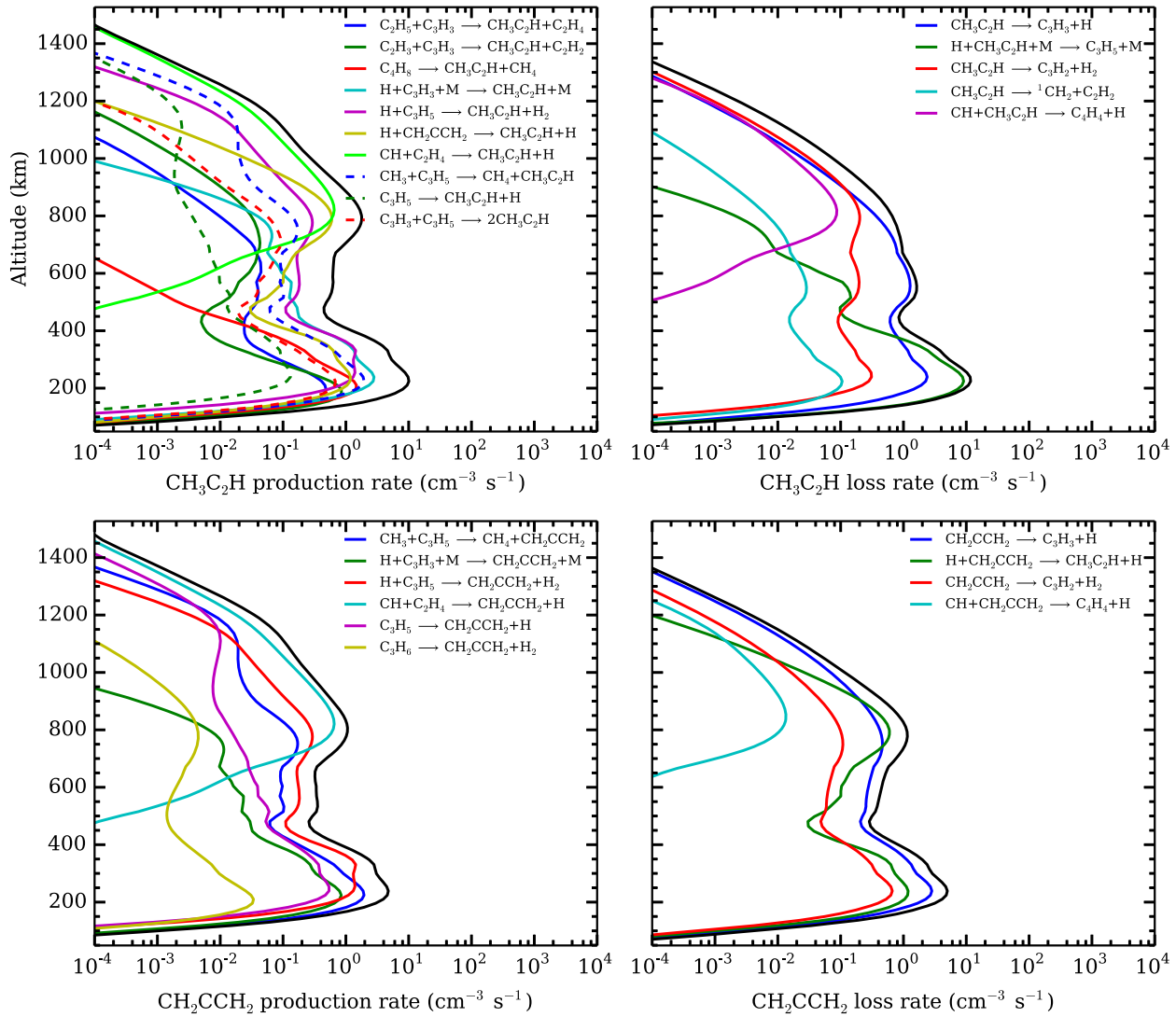

Figure 4. Production and loss rates of CH_3C_2H and CH_2CCH_2 due to reactions listed in the figure. The sum of the reactions accounts for more than 90% of the total production and loss rates at each altitude. The total production and loss rates are given by the black lines.

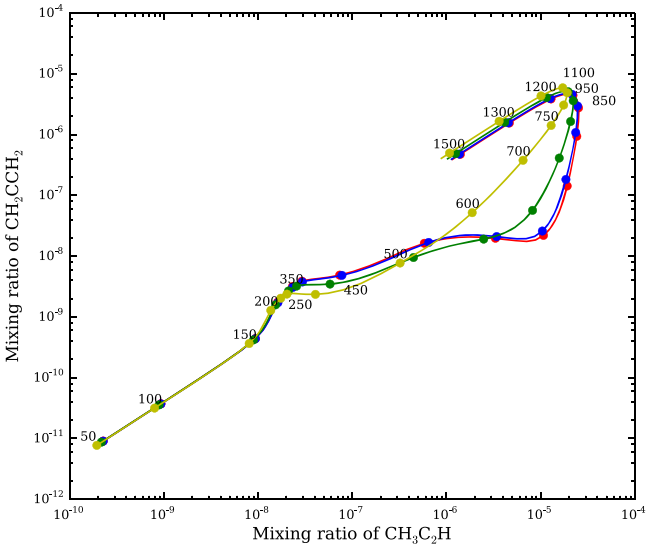

Figure 5. Correlation between CH_3C_2H and CH_2CCH_2 with accommodation coefficients of 0 (red), 0.001 (blue), 0.01 (green), and 0.1 (yellow) for H on aerosol particles. The numbers labeling the points indicate the altitude in Titan's atmosphere in km.

that further analysis of *Cassini*/CIRS limb-view observations combined with better laboratory constraints on the spectra of CH_2CCH_2 will lead to its detection, which would fill another gap in the C_3-hydrocarbon family. The observed mixing ratio of CH_3C_2H is 10^{-8}, while our calculated mixing ratio for CH_2CCH_2 in the stratosphere is about 10^{-9}. Confirmation or rejection of this value requires improved laboratory spectral data. Finally, c-C_3H_6 is not likely to be observed due to its low abundance ($\sim 10^{-11}$).

This research was supported in part by NASA grants NNX09AB72G and *Cassini* UVIS program grant JPL.1459109 to the California Institute of Technology. X.Z. was supported by the Bisgrove Scholar Program at the University of Arizona. Y.L.Y. was supported in part by the NAI on Titan Astrobiology.

REFERENCES

Coustenis, A., Achterberg, R. K., Conrath, B. J., et al. 2007, Icar, 189, 35
Coustenis, A., Salama, A., Schulz, B., et al. 2003, Icar, 161, 383
Fulchignoni, M., Ferri, F., Angrilli, F., et al. 2005, Natur, 438, 785
Galland, N., Caralp, F., Hannachi, Y., et al. 2003, JPCA, 107, 5419

Goulay, F., Trevitt, A. J., Meloni, G., et al. 2009, JAChS, 131, 993
Hebrard, E., Dobrijevic, M., Loison, J. C., et al. 2013, A&A, 552
Kammer, J. A., Shemansky, D. E., Zhang, X., & Yung, Y. L. 2013, P&SS, 88, 86
Koskinen, T. T., Yelle, R. V., Snowden, D. S., et al. 2011, Icar, 216, 507
Krasnopolsky, V. A. 2009, Icar, 201, 226
Krasnopolsky, V. A. 2010, P&SS, 58, 1507
Krasnopolsky, V. A. 2014, Icar, 236, 83
Lavvas, P., Sander, M., Kraft, M., & Imanaka, H. 2011, ApJ, 728, 80
Lavvas, P. P., Coustenis, A., & Vardavas, I. M. 2008a, P&SS, 56, 27
Lavvas, P. P., Coustenis, A., & Vardavas, I. M. 2008b, P&SS, 56, 67
Li, C., Zhang, X., Kammer, J. A., et al. 2014, P&SS, 104, 48
Loison, J. C., Hébrard, E., Dobrijevic, M., et al. 2015, Icar, 247, 218
Magee, B. A., Waite, J. H., Mandt, K. E., et al. 2009, P&SS, 57, 1895
Moses, J. I., Fouchet, T., Bezard, B., et al. 2005, JGRE, 110, E08001
Navarro-González, R., & Ramírez, S. I. 1997, AdSpR, 19, 1121
Niemann, H. B., Atreya, S. K., Bauer, S. J., et al. 2005, Natur, 438, 779
Nixon, C. A., Achterberg, R. K., Teanby, N. A., et al. 2010, FaDi, 147, 65
Nixon, C. A., Jennings, D. E., Bezard, B., et al. 2013, ApJL, 776, L14
Roe, H. G., Greathouse, T., & Tokunaga, A. 2011, in EPSC-DPS Joint Meeting (Göttingen, Germany: Copernicus), 1398
Rogers, D. W., & Mclafferty, F. 1995, JPhCh, 99, 1375
Sekine, Y., Imanaka, H., Matsui, T., et al. 2008a, Icar, 194, 186
Sekine, Y., Lebonnois, S., Imanaka, H., et al. 2008b, Icar, 194, 201
Vinatier, S., Bezard, B., Nixon, C. A., et al. 2010, Icar, 205, 559
Vuitton, V., Yelle, R. V., Lavvas, P., & Klippenstein, S. J. 2012, ApJ, 744, 11
Vuitton, V., Yelle, R. V., & McEwan, M. J. 2007, Icar, 191, 722
Westlake, J. H., Bell, J. M., Waite, J. H., et al. 2011, JGRA, 116, A03318
Wilson, E. H., & Atreya, S. K. 2004, JGRE, 109, E06002
Wilson, E. H., & Atreya, S. K. 2009, JPCA, 113, 11221
Yelle, R. V., Cui, J., & Muller-Wodarg, I. C. F. 2008, JGRE, 113, E10003
Yung, Y. L., Allen, M., & Pinto, J. P. 1984, ApJS, 55, 465